

ORIGINAL
RESEARCH

L.M. Nagae
A.H. Hoon, Jr.
E. Stashinko
D. Lin
W. Zhang
E. Levey
S. Wakana
H. Jiang
C.C. Leite
L.T. Lucato
P.C.M. van Zijl
M.V. Johnston
S. Mori

Diffusion Tensor Imaging in Children with Periventricular Leukomalacia: Variability of Injuries to White Matter Tracts

BACKGROUND AND PURPOSE: Conventional MR imaging shows evidence of brain injury and/or maldevelopment in 70%–90% of children with cerebral palsy (CP), though its capability to identify specific white matter tract injury is limited. The great variability of white matter lesions in CP already demonstrated by postmortem studies is thought to be one of the reasons why response to treatment is so variable. Our hypothesis is that diffusion tensor imaging (DTI) is a suitable technique to provide in vivo characterization of specific white matter tract lesions in children with CP associated with periventricular leukomalacia (PVL).

MATERIALS AND METHODS: In this study, 24 children with CP associated with PVL and 35 healthy controls were evaluated with DTI. Criteria for identification of 26 white matter tracts on the basis of 2D DTI color-coded maps were established, and a qualitative scoring system, based on visual inspection of the tracts in comparison with age-matched controls, was used to grade the severity of abnormalities. An ordinal grading system (0 = normal, 1 = abnormal, 2 = severely abnormal or absent) was used to score each white matter tract.

RESULTS: There was marked variability in white matter injury pattern in patients with PVL, with the most frequent injury to the retrolenticular part of the internal capsule, posterior thalamic radiation, superior corona radiata, and commissural fibers.

CONCLUSION: DTI is a suitable technique for in vivo assessment of specific white matter lesions in patients with PVL and, thus, a potentially valuable diagnostic tool. The tract-specific evaluation revealed a family of tracts that are highly susceptible in PVL, important information that can potentially be used to tailor treatment options in the future.

The term cerebral palsy (CP) describes motor impairment attributable to early injury to the developing brain, encompassing pre-, peri-, and postnatal etiologies.^{1,2} Periventricular leukomalacia (PVL) refers to the most common brain injury in premature neonates, related to the susceptibility of the periventricular white matter to focal ischemic and/or infectious/inflammatory destructive processes occurring between 24 and 34 weeks of gestation.³ A more diffuse noncystic injury to immature oligodendrocytes is now increasingly recognized in infants discharged from modern neonatal intensive care units.^{3,4} Associated abnormalities may include reductions in cortical gray matter, deep gray matter and posterior fossa injury.⁵⁻⁷

Neuropathologic data reveal coagulative necrosis in the periventricular white matter with diffuse glial injury or focal

injuries that can potentially cavitate.⁸⁻¹⁰ MR imaging techniques, including MR imaging, diffusion-weighted MR imaging (DWI), and diffusion tensor imaging (DTI), have been established as the imaging techniques of choice for initial characterization and follow-up of these patients.^{7,11-15} Typical MR imaging findings in childhood show enlarged ventricular atria and volume loss in periventricular white matter, often associated with T2 and fluid-attenuated inversion recovery (FLAIR) hyperintense signal intensity and, more rarely, with cysts.¹⁵ However, assessment of injuries to specific white matter tracts has been difficult with conventional MR imaging.

DTI has been well studied in normal brain development¹⁶⁻¹⁸ and has been shown to improve detection of lesions in the first years of life.¹⁹⁻²¹ Results have provided further understanding of pathogenesis and treatment in a range of neurologic disorders by providing visualization of specific white matter fiber tracts (see review by Horsfield and Jones²²).²³⁻²⁷ Although injury to the corticospinal tracts is thought to be the major determinant of motor impairment in children with PVL, recent studies have shown that sensory pathways, including the posterior thalamic radiation, may be affected instead or, concurrently,²⁸ indicative of the complexity of white matter involvement in PVL.^{29,30}

Criteria for DTI-based identification of various white matter tracts at 26 locations were established and applied to 24 children with CP associated with PVL as well as in a group of 35 unaffected controls to further elucidate the diversity of white matter tract injury involvement in PVL. A qualitative scoring system, based on visual inspection of the white matter tracts, was used to describe the status of the various white matter tracts.

Received May 31, 2005; accepted after revision December 18, 2006.

From The Russell H. Morgan Department of Radiology and Radiological Science (L.M.N., H.J., P.C.M.v.Z., D.L., S.M.), Johns Hopkins University School of Medicine, Baltimore, Md; the Kennedy Krieger Institute (L.M.N., A.H.H., E.S., M.V.J., W.Z., E.L., S.W., P.C.M.v.Z., S.M.), Johns Hopkins University, Baltimore, Md; Hospital das Clínicas da Faculdade de Medicina da Universidade de São Paulo (L.M.N., C.C.L., L.T.L.), São Paulo, Brazil; and Hospital Israelita Albert Einstein (L.M.N.), São Paulo, Brazil.

This work was supported by the National Institutes of Health (NIH) grant R01 AG20012, P41 R15241, the Dana Foundation Clinical Hypothesis Program in Imaging, the United Cerebral Palsy Research and Educational Foundation, the National Center for Research Resources (NCRR), and the Johns Hopkins University School of Medicine General Clinical Research Center. Grant #M01-RR00052 from the NCRR/NIH. Dr. van Zijl is a paid lecturer for Philips Medical Systems. This arrangement has been approved by Johns Hopkins University in accordance with its conflict of interest policies.

Paper previously presented at: Annual Meeting of the American Society of Neuroradiology, May 2005; Toronto, Ontario, Canada.

Please address correspondence to Lidia M. Nagae, MD, Av. Albert Einstein 701, Bloco D, 4 andar Morumbi, São Paulo, CEP 05651-901 Brazil; e-mail: lidiamayumi@gmail.com

DOI 10.3174/ajnr.A0534

Subjects and Methods

Patients

As part of an ongoing larger DTI study of childhood CP, 37 patients with CP were consecutively scanned. Criteria for enrollment in the study were the following: 1) children aged birth to 18 years, 2) diagnosis of CP, and 3) a clinically indicated brain scan (for diagnosis or follow-up). This study focused on a subsample of 24 children born at fewer than 37 weeks gestation with PVL diagnosed by neuroradiologic review of conventional MR imaging. There were 14 boys and 10 girls in this study group, ranging in age from 16 months to 13 years 3 months, with a mean age of 6 years. Gestational age at birth ranged from 23 to 34 weeks (mean, 29 weeks). Most children had spastic diplegia (18/24, 75%); 3, spastic quadriplegia; 2, hemiplegia; and 1, ataxic CP with hypotonia.

Informed consent was obtained from the parents or guardians, and the protocol was approved by the institutional review board. The DTI research protocol was preceded by a conventional MR imaging with standard imaging protocol. A neuroradiologist not involved in the study interpreted the conventional images, which were reviewed with the family. Most patients (32/34) required sedation for the conventional clinical images and remained sedated for the DTI research images.

Normative data for age-matched controls were obtained from 35 children from our pediatric DTI de-identified data base (cmrm.med.jhmi.edu). Controls were distributed in the age ranges of 12–23 months (5 toddlers), 2–3 years (11 children), 4–5 years (5 children), 6–8 years (6 children), 10 years (2 children), and 12–15 years (6 teenagers).

Imaging Protocol

Data were obtained at a 1.5T scanner (ACS-NT; Philips Medical Systems, Best, the Netherlands). Initially, all patients had routine clinical pulse sequences, including sagittal (4-mm section thickness, 1-mm intersection gap) and axial (4-mm section thickness, no intersection gap) T1-weighted (TR/TE, 297.07–598.87/10.5–13 ms), fat-saturated axial T2-weighted (TR/TE, 3992.36–4524.67/110 ms), and FLAIR (TR/TI/TE, 6000/2000/120 ms) sequences.

DTI was acquired following the clinical sequences and consisted of a diffusion-weighted spin-echo pulse sequence with a single-shot echo-planar imaging readout with TR ranging from 6.2 to 9.4 seconds and TE of 80 ms. Fifty axial sections parallel to the anterior/posterior commissure line were acquired, covering the entire brain. The maximal b-value was 700 seconds/mm², used in a 30 different gradient-direction scheme along with 5 reference images with minimal diffusion-weighting.³¹ Spin-echo acquisition and sensitivity encoding (SENSE) was used, with an 8-element phased-array coil, converted to a 6-channel coil to be compatible with a 6-channel receiver, with a SENSE reduction factor (R) of 2.5. FOV was adjusted to the brain size, and the imaging matrix was changed within a range of 80 × 80 to 96 × 96, resulting in in-plane imaging resolution of 2.0–2.5 mm. All images were zero-filled to a 256 × 256 matrix. Section thickness was set to approximately the same as that in the in-plane resolution. Scanning times varied from 4 minutes 18 seconds to 6 minutes 34 seconds per sequence. Three repetitions were performed to increase signal intensity-to-noise ratio.

3D-magnetization-prepared rapid acquisition of gradient echo (MPRAGE) images were also obtained with the same section localization, number, and thickness as well as the same FOV of DTI, TR/TE/flip angle of 6.8–8.8/3.3–3.7 ms/8°, scan duration of 3 minutes, and R = 2.5.

Postprocessing

All DTI acquisition datasets were transferred to a workstation and corrected for bulk motion by using the automated imaging registration program.³² DTI postprocessing was performed by using DtiStudio (free software available at <http://cmrm.med.jhmi.edu>) (H.J. and S.M., Johns Hopkins University, Baltimore, Md) and included generation of fractional anisotropy (FA), vector maps, and color-coded maps.^{33–35} The processing algorithm used assumed that the eigenvector associated with the largest eigenvalue represented the average main fiber orientation of a particular pixel. In the color-coded maps, colors were assigned according to the vector map as blue representing superior-inferior orientation (through the axial plane); green, antero-posterior orientation; and red, laterolateral orientation. Tracts with oblique angles were represented with the appropriate mixture of these basic colors. Color intensity was scaled proportional to FA values.

White Matter Tract Identification

White matter tract identification was performed by using the color-coded maps, with specific criteria listed in Fig 1.^{35–39} Two- and 3D representations of some of the tracts can also be found in our previous publication in more detail.³⁷

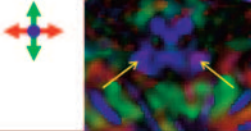
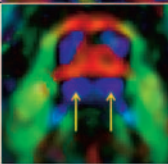
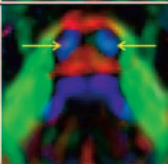
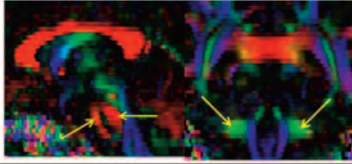
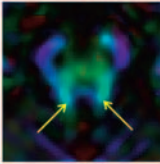
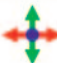
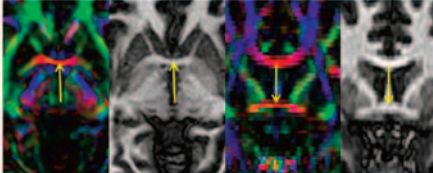
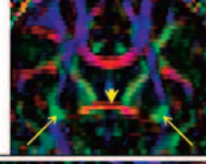
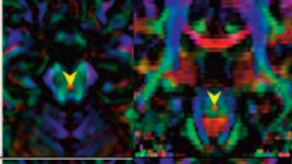

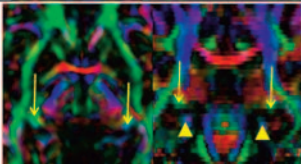
Although tracts were identified primarily by the color-coded maps, MPRAGE was also used to supplement interpretation, especially for the corpus callosum, anterior commissure at the midsagittal level, and the column and body (superior part) of the fornix. These fiber tracts can be discretely identified by MPRAGE, which offers higher resolution to assess their anatomy.

Structures that benefit the most from identification on color-coded maps include projectional fibers such as the corona radiata, anterior thalamic radiation, sagittal stratum, posterior thalamic radiation, retrolenticular part of the internal capsule, and association fibers such as the superior longitudinal fasciculus, inferior fronto-occipital fasciculus, uncinate fasciculus, and inferior longitudinal fasciculus. These tracts cannot be individually identified on conventional MR imaging because they are intermingled. Color-coded maps, carrying orientation information, can separate individual tracts. Other structures identified on conventional imaging such as the corticospinal/corticopontine tracts; medial lemniscus; middle, inferior, and superior cerebellar peduncles; and cingulum also benefit from more precise delineation on the color maps. Color maps reveal a range of different colors in the inner architecture of the cerebral peduncles and thalami, showing more details of these structures.

Scoring System

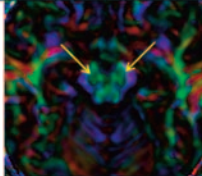
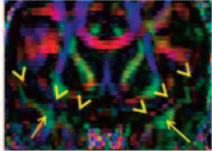
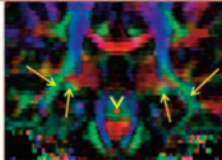
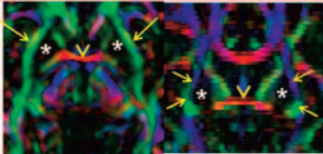
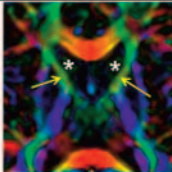

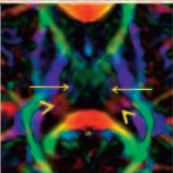
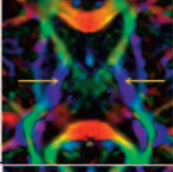
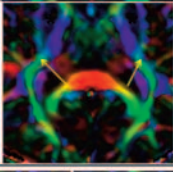
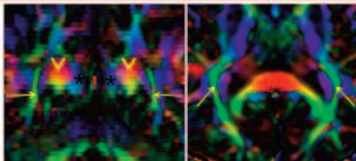
Once these tracts were identified on the basis of the protocol described in Fig 1, an evaluation was completed by using all 3 orthogonal planes of the interactive viewer in DTIStudio. An ordinal grading system (0 = normal, 1 = abnormal, 2 = severely abnormal or absent) was used by the primary study rater (L.M.N.) to score each tract. Abnormalities of the white matter tracts were based on size reduction on visual inspection in comparison with age-matched controls, in whom white matter tracts were all scored 0. The recognition that a significant decrease of diffusion anisotropy could lead to the appearance of a smaller tract size and thus be scored as abnormal was considered in the interpretation. If size reduction of the tract was identified, the tract was scored as abnormal (score 1). A questionable abnormality was conservatively scored as normal. A structure absent or so abnormal that it could hardly be identified was characterized as severely abnormal or absent (score 2).

To assess inter-rater reliability, 2 experienced neuroradiologists

fiber	localization	representative images	description
inferior cerebellar peduncles (icp)	I-a		On the axial slice at the most rostral medulla level where the mcp is still not evident, 2 pairs of rounded blue fibers are identified. The icp are the posteriorly located pair of fibers.
ascending sensory tract (ast)	I-b		The ast includes the medial lemniscus, central tegmental tract, and medial & dorsal longitudinal fasciculi. Evaluation includes all pons levels (3-4 slices) where the posterior, well-defined bilateral blue oval structure is identified.
corticopontine/ corticospinal tracts (cpt/cst)	I-c		Evaluation includes all pons levels (5-6 slices) where the anterior pair of blue fibers are identified.
middle cerebellar peduncles (mcp)	II-a		The medial fibers of the mcp (red crossing fibers) are evaluated at the pons level on the mid-sagittal slice. On the coronal plane, the mcp is the round-shaped green fiber bundle lateral to the pons. This slice is obtained as the orthogonal plane of the medial lemniscus on an axial slice.
superior cerebellar peduncles (scp)	I-d		The scp is identified as the cyan blue tracts on the axial plane, on the slice right above the red crossing pontine fibers.
Anterior commissure (ac)	 I-e I-f		On the midsagittal plane, identify the red dot inferior and posterior to the rostrum of the corpus callosum to obtain the ac on the correspondent axial and coronal planes.
uncinate/inferior fronto-occipital tracts (unc/ifo)	I-f		On the coronal slice, at the level of the anterior commissure, identify the cross-sectioned pair of green fiber bundles lateral to the anterior commissure (arrow head).
decussation of the superior cerebellar peduncles (dscp)	I-g I-h		On the midsagittal plane, identify the red dot in the brainstem to obtain the dscp on the correspondent axial and coronal planes.
Inferior cingulum (icg)	I-g I-h		At the level of the decussation of the superior cerebellar peduncles (arrow head) on the axial slice, identify a pair of bluish/cyan blue fiber bundles lateral to the cerebral peduncles. The icg is also evaluated on the coronal and sagittal planes.
Inferior fornix or crus fornicis (ifx)	I-e		On the axial slice, at the level of the anterior commissure, identify the cross-sectioned pair of greenish/bluish fiber adjacent to the cerebral peduncles. The coronal plane obtained at the ifx reveals this bundle located superior to the icg (arrow heads).


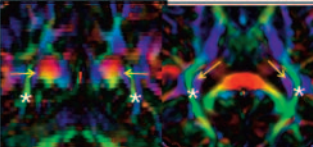
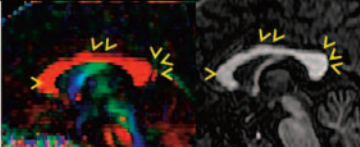
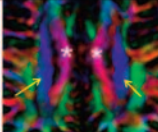
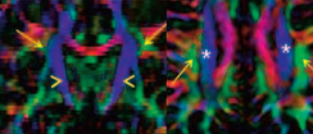
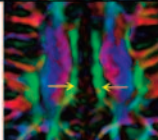

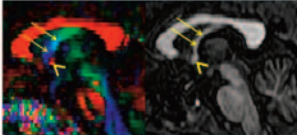
A

Fig 1. A, Description of the white matter tract identification protocol. Representative color-coded map or MPRAGE images are shown along with localization in a reference image (B).

fiber	localization	representative images	description
Cerebral peduncle (cp)	II-b		Evaluation includes all midbrain levels (6-7 slices).
uncinate/inferior longitudinal fasciculi (unc/ilf)	I-j		On the coronal slice, at the most posterior level where the temporal lobes can be seen separated from the frontal lobes by the Sylvian fissure (arrow heads), identify the green fiber bundle in the temporal lobe.
Inferior fronto-occipital/inferior longitudinal fasciculi (ifo/ilf)	I-h		Green fiber bundles identified on the coronal slice at the level of the dscp (arrow head), lateral to the ifx (thin arrows).
External capsule (ec)	I-e I-f		At the level of the ac (arrow head) on the axial slice, identify a pair of green (inferiorly) and blue (superiorly) fiber bundles lateral to the lentiform nucleus (asterisk). The coronal slice reveals green and blue fibers in the ec.
Anterior limb of the internal capsule (alic)	II-c		Evaluation includes all axial levels (6-7 slices) where the green bundles lateral to the head of the caudate nucleus (asterisk) can be seen.
Superior fronto-occipital fasciculus/anterior thalamic radiation (sfo/atr)	III-a		Evaluation includes cross-sectional coronal views of the green fiber bundles corresponding to the alic in all slices seen.
thalamus (tha)	I-j		Evaluation includes all axial levels (6-7 slices) where the thalamus can be seen with a greenish and a redish portions (arrow heads).
posterior limb of the internal capsule (plic)	II-c		Evaluation includes all axial levels (6-7 slices) where the blue fibers lateral to the thalamus (asterisk) can be seen.
Retrolenticular part of the internal capsule (rlc)	II-d		Evaluation includes all axial levels (6-7 slices) where the green fibers posterior to the lentiform nucleus (asterisk) can be seen.
Posterior thalamic radiation (ptr)	II-e II-d		Starting from a parasagittal plane (II-e), a coronal plane is obtained at the level of the posterior cingulum (asterisk). The ptr is identified as a pair of prominent green fiber bundles lateral to the cc (arrow heads).

A

Fig 1 continued

fiber	localization	representative images	description
Tapetum (tap)	II-e 		Blue fibers medial to the ptr (asterisk).
Corpus callosum (cc) Genu, body & splenium	IV-a		On the midsagittal slice, the cc can be evaluated separately as the genu (arrow head), body (double arrow head) and splenium (triple arrow head).
Superior corona radiata (scr)	II-f		On the axial slice, at the level where the corpus callosum is separated at the midline (asterisk), the scr can be identified as a pair of blue fiber bundles.
superior longitudinal fasciculus (slf)	III-b		Triangular green fiber bundles identified on the coronal slice at the level of the middle of the plic (arrow heads). On the axial slice, it is identified as a pair of green fiber bundles lateral to the scr (asterisk).
Superior cingulum (scg)	IV-b		Evaluation includes all axial levels (3-4 slices) where the scr can be seen as a pair of medially located green fiber bundles. On the coronal images, the scr is located superior to the cc, close to the midline.
Superior fornix (sfx)	IV-a 		Bluish/greenish oblique elongated structure at the midsagittal slice, anterior to the ac (arrow head).

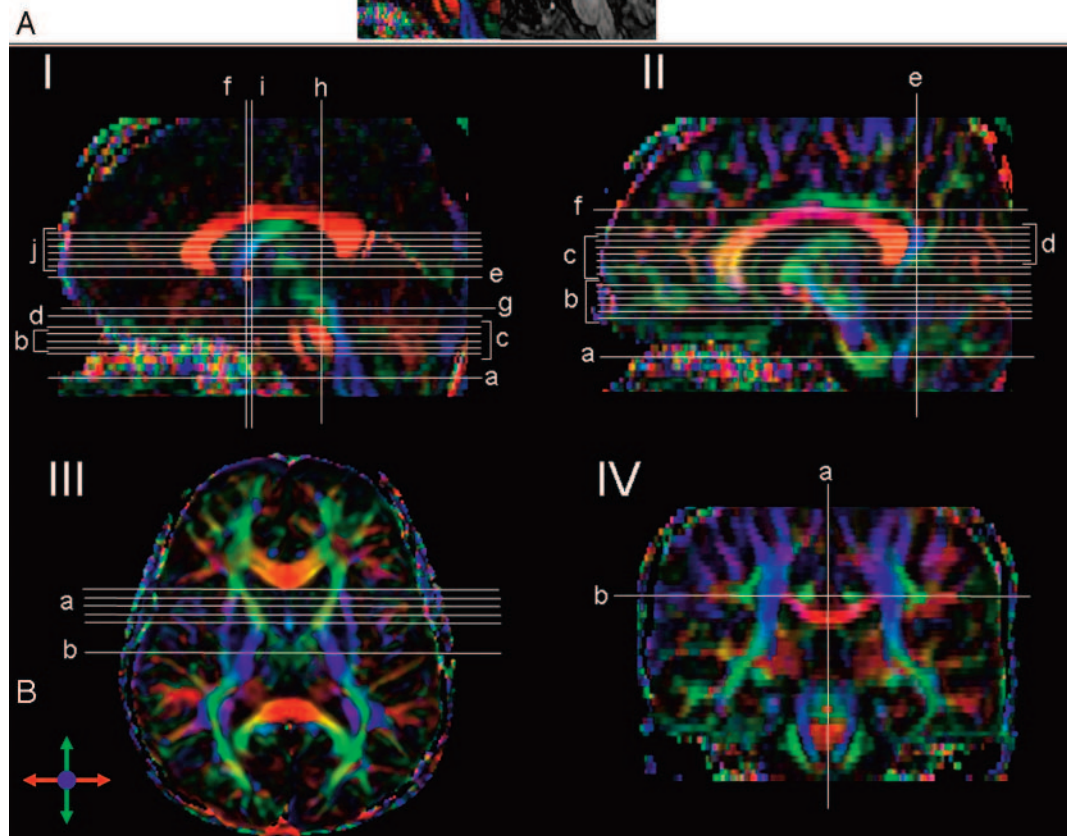


Fig 1 continued

(D.L., W.Z.) scored the study data independently, masked to clinical information on the patients. The 2 raters received instructions as described in this article regarding the structures to be scored and the control dataset. To establish intrarater reliability estimates for the white matter tract grading, the primary rater (L.M.N.) repeated the tract scoring, and observations at times 1 and 2 were compared. Percentage of agreement was used to rate intra- and inter-rater reliability of this grading system.

Fiber Tracking

Fiber tracking was performed by using DTIStudio, which uses the fiber-assignment continuous tracking approach.⁴⁰ By combining information from FA and vector maps, this approach allows 3D reconstruction of fibers in a continuous vector field. The threshold chosen for FA was 0.15 and the angle threshold, 60°. These thresholds were lower than those used in our previous articles^{36,40} due to partial volume effects between structures of the brain and the lower FA of white matter in pediatric brains compared with those of adults. The initial tracking was started from a region of interest drawn on the color-coded orientation maps. A “brute force” approach^{41,42} was used, in which fiber tracking was initiated from all pixels, and tracking results that penetrated the region of interest were included. A multiple region of interest reference scheme was used, including “AND” and “NOT” operations: “AND” operation, restricting the tracking to only the fibers that penetrate both regions of interest, and “NOT” operation, excluding fibers within the respective region of interest.^{37,38}

To demonstrate the variability of white matter tract injury in PVL, we constructed 2 fiber tracts in 3 children. To demonstrate the relatively preserved tracts in the posterior limb of the internal capsule, we drew one region of interest on the posterior limb of the internal capsule, yielding tracking of all the fibers penetrating this structure. To illustrate injury to the posterior thalamic radiation, the major constituent of the retrolenticular part of the internal capsule, which is often severely affected in PVL, we drew 2 regions of interest. The first region of interest was drawn in the coronal plane, cross-sectioning the retrolenticular part of the internal capsule, and the second region of interest defined the thalamus. An AND operation selected the fibers passing through both regions of interest. For both the posterior limb of the internal capsule and the posterior thalamic radiation reconstruction, fibers that apparently were not related to the tracts of interest, such as the corpus callosum and the anterior limb of the internal capsule, were rejected by using a NOT operation.

Results

In this study sample of children with PVL, 19 tracts were graded as abnormal by using the 0–2 scoring system. The qualitative examination revealed striking differences between the posterior limb of the internal capsule and the retrolenticular part of the internal capsule/posterior thalamic radiation tracts, in terms of the frequency and degree of injuries.

Some examples of affected tracts and of the grading results, including the corticopontine/corticospinal tracts, posterior limb of the internal capsule, retrolenticular part of the internal capsule, posterior thalamic radiation, inferior fronto-occipital/inferior longitudinal fasciculi, superior longitudinal fasciculus, superior corona radiata, and the corpus callosum, are shown in Fig 2. For the posterior limb of the internal capsule, no example for score 2 (most severe) was found in this patient population. Histograms of frequency of scores for the illustrated individual tracts are also shown in Fig 3.

As a visual support for the trajectories of the affected fibers, the white matter tracts were reconstructed in 3D in three 7-year-old children, including 1 healthy control and 2 patients with PVL (Fig 4). One of the patients (Fig 4B) displayed relative preservation of the fibers penetrating the posterior limb of the internal capsule (score 0) and reduced fibers in the posterior thalamic radiation (score 1). Figure 4C shows a second child in whom the posterior thalamic radiation fibers are more severely affected (score 2). In this example, it can be clearly seen that the corona radiata is also affected (score 2).

Other white matter tracts that were frequently affected included the corticopontine/corticospinal tracts and the corpus callosum, whereas association fibers and limbic fibers (fornix [left side: score 1 = 2 cases (8.3%)] and cingulum [right side: score 1 = 2 cases (8.3%); left side: score 1 = 4 cases (16.6%)]) were relatively more preserved. In agreement with the lesions seen in the retrolenticular part of the internal capsule and posterior thalamic radiation, abnormalities of the corpus callosum were most often seen along the body and splenium of the corpus callosum. The tapetum, believed to be a part of temporal commissural fibers, was affected in most patients as well (right side: score 2 = 16 cases [66%], score 1 = 4 cases [16.6%], score 0 = 4 cases [16.6%]; left side: score 2 = 18 cases [75%], score 1 = 3 cases [12.5%], score 0 = 3 cases [12.5%]).

Prominent sensory tracts in the brain stem (medial lemniscus) were all scored 0 in this population of patients (images not shown). The cerebellar peduncles, which include sensory and motor fibers, were affected in 8/24 patients (score 1, 33.3%).

Percentage agreement was used as a first step to rate inter-rater reliability of this grading system. On a 3-point scale (0, 1, 2) percentage agreement between the 2 additional raters was 78%. Reducing the categories to a 2-point scale (normal/abnormal) improved inter-rater agreement to 84%. Both are acceptable. Percentage scoring agreement between the 2 raters and the primary study rater ranged from 0.68 to 0.73 agreement on the 3-point scale and 0.77–0.79 on a normal/abnormal rating scale. Intrarater reliability estimates for the primary study rater (observations 1–2) were 86% agreement; intrarater agreement improved to 91% on a 2-point scale (normal/abnormal 1). The percentage agreement reported represented an average of comparisons across all white matter tracts scored. In fact, with the 3-point qualitative scoring system, there was 90%–100% agreement among all 3 raters on selected tracts: cerebral peduncles; middle cerebellar peduncles, sagittal view; inferior fronto-occipital/inferior longitudinal fasciculus; superior fronto-occipital fasciculus; posterior limb of the internal capsule; thalamus; uncinate/inferior fronto-occipital fasciculus; and inferior cingulum.

Discussion

Despite a wide range of medical interventions in children with CP, there is significant variability in outcome,^{43–46} related in part to the heterogeneous nature of the underlying brain pathology. Findings in this study demonstrate the utility of DTI in characterizing injury in specific white matter tracts in children with PVL, a capability beyond that possible on conventional MR imaging.^{23,28,29,47}

In this study, we used the DT-generated color-coded maps to classify the status of major white matter tracts by using a

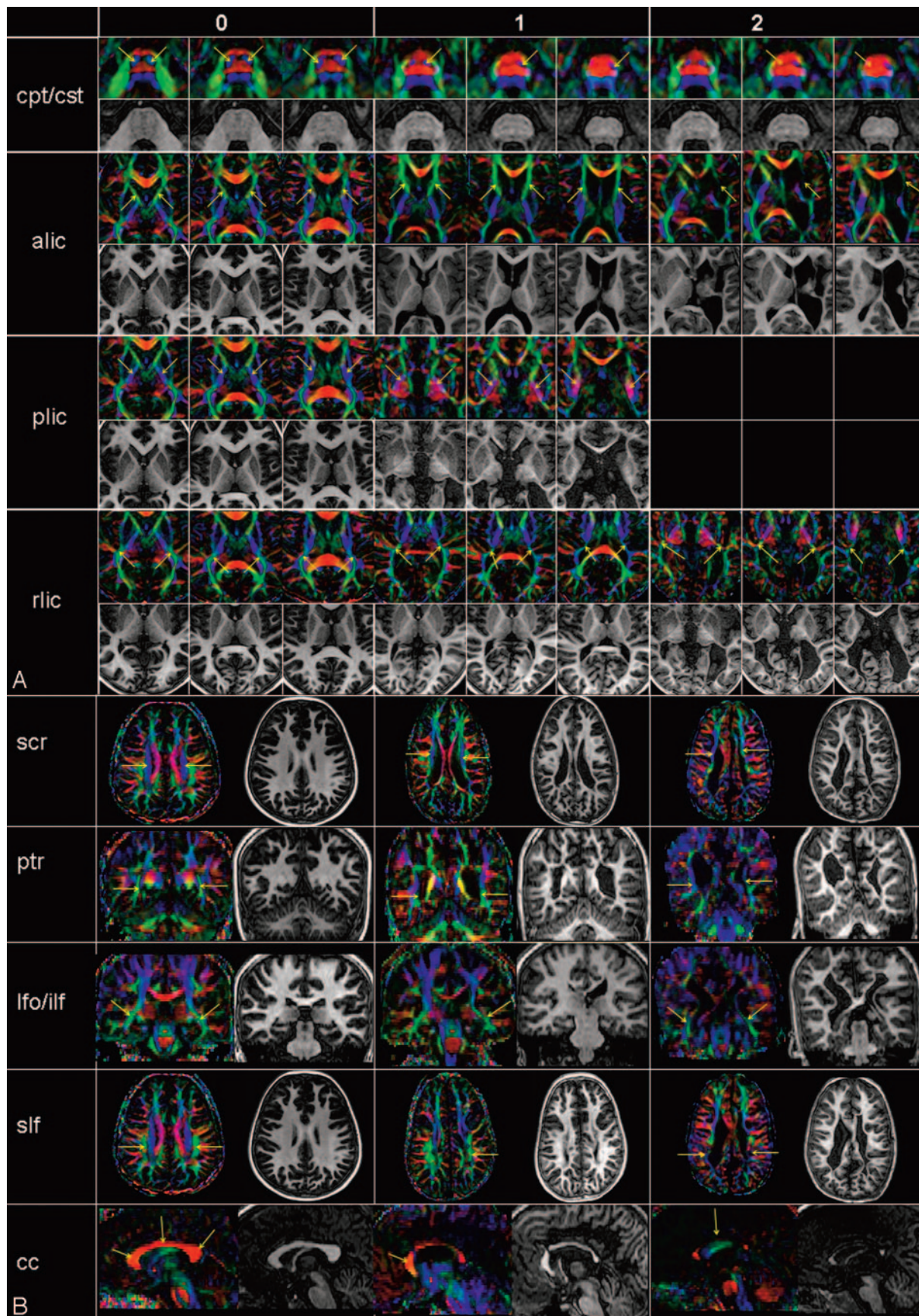


Fig 2. A and B, Examples of the scoring system obtained from a 7-year-old healthy control (score 0) and patients with PVL (scores 1 and 2). See Fig 1 for abbreviations.

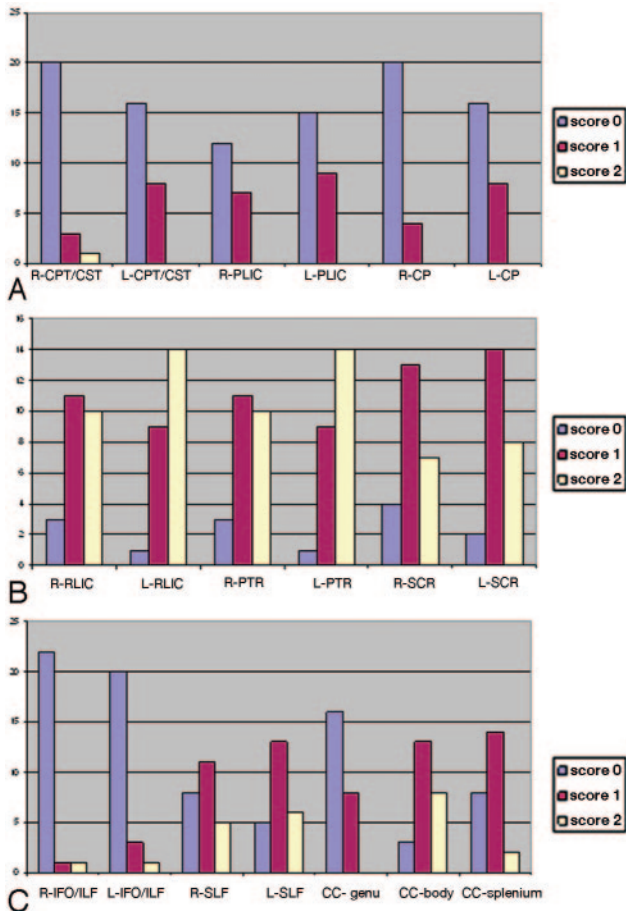


Fig 3. Histogram of frequency of scores for individual tracts. *A*, tracts predominately related to motor pathways; *B*, tracts predominately related to sensory motor pathways; and *C*, association and commissural fibers. L indicates left; R, right; CPT/CST, corticopontine/corticospinal tracts; PLIC, posterior limb of the internal capsule; CP, cerebral peduncles; RLIC, retrolenticular part of the internal capsule; PTR, posterior thalamic radiation; SCR, superior corona radiata; IFO/ILF, inferior fronto-occipital/inferior longitudinal fasciculi; SLF, superior longitudinal fasciculus; CC-genu, corpus callosum-genu; CC-body, corpus callosum-body; CC-splenium, corpus callosum-splenium.

3-grade system based on a qualitative visual assessment of each individual white matter tract. The color-coded map, combined with conventional T1-weighted images, allowed detailed assessment of white matter anatomy of the patients. Our results confirmed that, even in such a small sample, there is high variability of injury to white matter.

Although qualitative evaluation of images carries a high degree of subjectivity, it reflects the daily activity in neuroradiology. The concept of using MR images of lesions in a scoring system has been shown to add great benefit for classification and follow-up studies.⁴⁸⁻⁵⁰ For valid scoring, it is imperative to know the normal range of anatomic variations. This is a particularly difficult task in children because normal anatomy changes during brain development, especially within the first years of life. In addition, the DTI-based color-coded maps are a relatively new technique, and dedicated training is needed for accurate differentiation between normal and abnormal.

Images considered as normal in this study were found in our control normative data base, including 35 age-matched healthy children from 12 months to 15 years of age. It has been an important present effort of our research group to obtain a large pool of DTI control data during brain development for

reference purposes and to learn the normal variability of white matter tracts in the healthy population in different stages of neurodevelopment. Because of the current limitations in our understanding of normal range, a qualitative grading system including only 3 different grades (0 = normal, 1 = abnormal, 2 = severely abnormal or absent) was adopted as a first approach to more objectively score the white matter tracts. One caveat of the present grading system is the potential insufficient sensitivity to lesion detection.

This study shows that multiple raters with guidelines can score white matter tracts visualized on DTI with moderate reliability. Although experienced neuroradiologists, the 2 raters participating in the reliability tests were given the criteria described in this study for white matter tract identification and scoring as well as the control data base, without formal training. Reducing the scoring to 2 categories (normal and abnormal) improved agreement across raters and scoring consistency of repeated observations within the primary rater (intrarater agreement).

Of note, there was variability in the scoring agreement among tracts—several tracts had 100% inter-rater agreement (cerebral peduncles, inferior fronto-occipital/inferior longitudinal fasciculus, superior fronto-occipital fasciculus). The lowest indexes for both intra- and inter-rater reliability tests performed were seen for the corpus callosum. This could be due to a wide variability in shape and size among different sexes and ages and, perhaps, any individual. This could also indicate that the color-coded maps, enhancing contrast along the edges of the corpus callosum, might have influenced its evaluation. Adding to what was discussed earlier, the corpus callosum might be one opposite case of low specificity to evaluation on color-coded maps.

Using a 2-scale grading system shows superior reliability results, and simply distinguishing between normal versus abnormal is important in both future clinical and research applications, with the idea that there is potential for a 3-scale grading system as we ourselves learn how to read the color-coded maps. Future studies including a larger number of patients with different degrees of severity might lead to a more refined grading system.

In our previous publication,²⁸ we reported 2 patients with PVL whose corticospinal tracts and fibers penetrating the posterior limb of the internal capsule were relatively well preserved, whereas the posterior thalamic radiation was severely affected. This was an unexpected observation because the fibers in the corticospinal tract and fibers penetrating the posterior limb of the internal capsule, which are related to motor functions, were expected to be one of the most affected tracts, whereas the posterior thalamic radiation, which connects the thalamus and parietal/occipital lobes and is mostly related to sensory function, was believed to be relatively preserved. In the current study, we observed that both the retrolenticular part of the internal capsule and the posterior thalamic radiation, in which thalamocortical/corticothalamic pathways are the major constituent, were the white matter tracts bearing the most frequent and severe injuries, replicating our previous report. These results are consistent with a previously reported pattern of lesions in PVL in postmortem data,⁵¹ and to the best of our knowledge, DTI is the first in vivo imaging technique capable of displaying such findings.

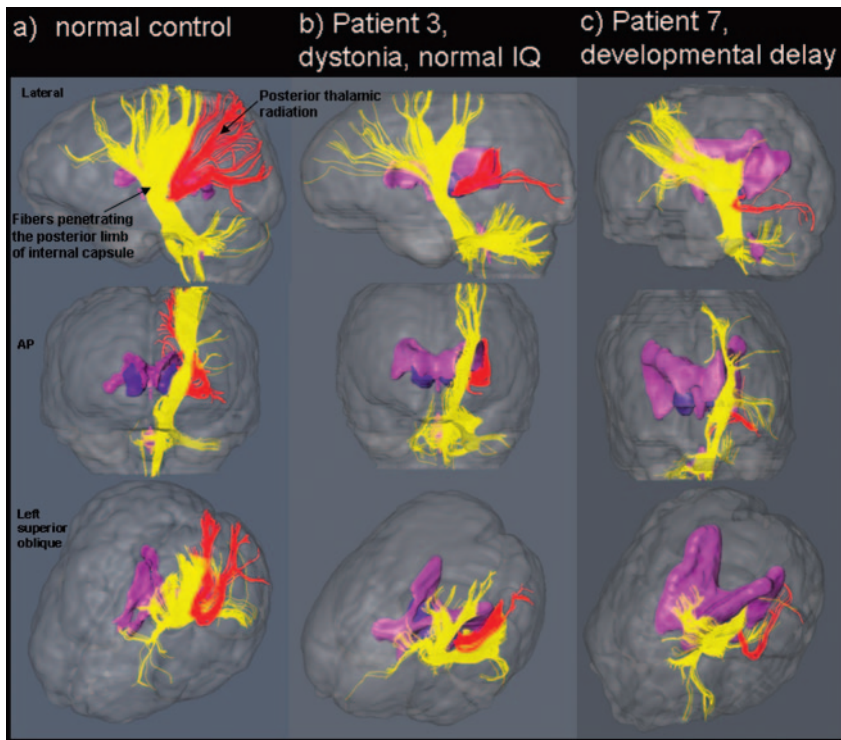


Fig 4. Examples of fiber tracking in 3 age-matched children. AP indicates anteroposterior.

One of the definite advantages of DTI is the possibility of quantitative measurement of tract diameters and tract-specific DTI parameters^{27,29,36,57,58} that will be attempted as a complementary study to the present one. However, one potential problem foreseen in these cases and previously discussed is partial volume effects due to the small brain size.

A 3D reconstruction (Fig 4) was used to visualize the fibers penetrating the posterior limb of the internal capsule and the posterior thalamic radiation. Although this technique is very powerful to visually understand the 3D trajectory of a tract of interest, its usefulness in routine diagnosis may be limited for several reasons. First, the reconstruction is strongly dependent on the location of the reference region of interest used for tracking and on subjective tract editing. Establishing strict protocols for region of interest placement could ameliorate these problems.^{36-38,58} However, establishment of a protocol can be challenging in patients with PVL, who often present with severe anatomic changes. Furthermore, the reconstruction results are affected by the 2 thresholds (FA and angle) for termination criteria. Although this effect could be potentially removed by using the same thresholds for all subjects, FA values for the white matter change during brain development,¹⁸ and the same FA threshold may not result in equivalent reconstruction results for brains with different ages, especially due to aforementioned partial volume effects. Therefore, use of 3D reconstruction may be limited for visual understanding of severe abnormalities found in color maps. For routine clinical practice, our belief is that 2D-based examination is an alternative suitable approach, promptly available for straightforward interpretation without extra processing time.

In summary, the variability in white matter injury in motor and sensory pathways can be clearly demonstrated with DTI. With the increased number of children studied and acquisition of additional control data, this technique will advance understanding of brain injury in children with childhood neurologic disorders, including CP. Our evaluation protocol is expected to be a guideline for routine clinical evaluation of patients with CP. The evaluation results provide clues to understand pathogenesis and may ultimately lead to improvements in clinical classification and treatment for children with CP and other neurologic disorders of childhood by providing specific treatment options based on the pattern of white matter injury.

Acknowledgments
We gratefully acknowledge the contributions of our research team: Heather Kammann, Terri Brawner, Kathleen Kahl, and Carolyn Gillen. We give special thanks to the families and children who participated in this study.

Important constituents of the retrolenticular part of the internal capsule/posterior thalamic radiation tracts, besides the thalamic pathways and the optic radiation, are long corticofugal pathways (most notably parieto-occipito-temporo-pontine tracts) and cortico-cortical association tracts such as the inferior longitudinal fasciculus and the inferior fronto-occipital fasciculus. Among these fibers, the association fibers were evaluated at different section levels (Fig 1) and were found to be relatively preserved in most patients.

The pontine tracts pass through the cerebral peduncles and are relayed to the middle cerebellar peduncles (corticoponto-cerebellar pathway) at the pons. Involvement of the cortico-pontine tracts in PVL is also possible, but the extent of abnormalities in the cerebral peduncles and the middle cerebellar peduncles was not as severe as that in the retrolenticular part of the internal capsule/posterior thalamic radiation.

It is also important to note that the corticospinal tracts were also often affected in our patient population, though the percentage of tracts scored as abnormal was higher for the retrolenticular part of the internal capsule and posterior thalamic radiation tracts than for the corticospinal tract. We also cannot exclude the possibility that the current grading protocol is not sensitive enough to specific loss of motor pathways responsible for functional deficits (as discussed previously).

Injuries of the commissural fibers were also prevalent in this patient population; this finding agrees with previous MR imaging observations of patients with PVL.⁵²⁻⁵⁶ Among the commissure fibers, the splenium of the corpus callosum and tapetum were most severely affected and are believed to contain commissural projections from the parietal, occipital, and temporal lobes. Combined with severe atrophy of the retrolenticular part of the internal capsule/posterior thalamic radiation, these results strongly suggest concentration of white matter injuries in the parietal and occipital white matter.

References

- Osler SW. *The Cerebral Palsies of Children*. London, UK: Mac Keith Press; 1987
- Keogh JM, Badawi N. The origins of cerebral palsy. *Curr Opin Neurol* 2006;19:129–34
- Volpe JJ. Cerebral white matter injury of the premature infant: more common than you think. *Pediatrics* 2003;112:176–80
- Miller SP, Cozzio CC, Goldstein RB, et al. Comparing the diagnosis of white matter injury in premature newborns with serial MR imaging and transfontanel ultrasonography findings. *AJNR Am J Neuroradiol* 2003;24:1661–69
- Folkerth RD. Neuropathologic substrate of cerebral palsy. *J Child Neurol* 2005;20:940–49
- Johnsen SD, Bodesnteinser JB, Lotze TE. Frequency and nature of cerebellar injury in the extremely premature survivor with cerebral palsy. *J Child Neurol* 2005;20:60–64
- Srinivasan L, Dutta R, Counsell SJ, et al. Quantification of deep gray matter in preterm infants at term-equivalent age using manual volumetry of 3-tesla magnetic resonance images. *Pediatrics* 2007;119:759–65
- Inder TE, Volpe JJ. Mechanisms of perinatal brain injury. *Semin Neonatol* 2000;5:3–16
- Rezaie P, Dean A. Periventricular leukomalacia, inflammation and white matter lesions within the developing nervous system. *Neuropathology* 2002;22:106–32
- Folkerth RD, Keefe RJ, Haynes RL, et al. Interferon-gamma expression in periventricular leukomalacia in the human brain. *Brain Pathol* 2004;14:265–74
- Huppi PS, Barnes PD. Magnetic resonance techniques in the evaluation of the newborn brain. *Clin Perinatol* 1997;24:693–723
- Counsell SJ, Rutherford MA, Cowan FM, et al. Magnetic resonance imaging of preterm brain injury. *Arch Dis Child Fetal Neonatal Ed* 2003;88:F269–274
- Huppi PS, Amato M. Advanced magnetic resonance imaging techniques in perinatal brain injury. *Biol Neonate* 2001;80:7–14
- Huppi PS, Inder TE. Magnetic resonance techniques in the evaluation of the perinatal brain: recent advances and future directions. *Semin Neonatol* 2001;6:195–210
- Barkovich AJ. Brain and spine injuries in infancy and childhood. In: Barkovich AJ, ed. *Pediatric Neuroimaging*. Philadelphia: Lippincott Williams & Wilkins; 2000:181–84
- Neil JJ, Shiran SI, McKinstry RC, et al. Normal brain in human newborns: apparent diffusion coefficient and diffusion anisotropy measured by using diffusion tensor MR imaging. *Radiology* 1998;209:57–66
- Mukherjee P, Miller JH, Shimony JS, et al. Diffusion-tensor MR imaging of gray and white matter development during normal human brain maturation. *AJNR Am J Neuroradiol* 2002;23:1445–56
- Mukherjee P, Miller JH, Shimony JS, et al. Normal brain maturation during childhood: developmental trends characterized with diffusion-tensor MR imaging. *Radiology* 2001;221:349–58
- Neil J, Miller J, Mukherjee P, et al. Diffusion tensor imaging of normal and injured developing human brain: a technical review. *NMR Biomed* 2002;15:543–52
- McKinstry RC, Miller JH, Snyder AZ, et al. A prospective, longitudinal diffusion tensor imaging study of brain injury in newborns. *Neurology* 2002;59:824–33
- Miller SP, Vigneron DB, Henry RG, et al. Serial quantitative diffusion tensor MRI of the premature brain: development in newborns with and without injury. *J Magn Reson Imaging* 2002;16:621–32
- Horsfield MA, Jones DK. Applications of diffusion-weighted and diffusion tensor MRI to white matter diseases: a review. *NMR Biomed* 2002;15:570–77
- Huppi PS, Murphy B, Maier SE, et al. Microstructural brain development after perinatal cerebral white matter injury assessed by diffusion tensor magnetic resonance imaging. *Pediatrics* 2001;107:455–60
- Hoon AH Jr, Belcito KM, Nagae-Poetscher LM. Neuroimaging in spasticity and movement disorders. *J Child Neurol* 2003;18(suppl 1):S25–39
- Glenn OA, Henry RG, Berman JJ, et al. DTI-based three-dimensional tractography detects differences in the pyramidal tracts of infants and children with congenital hemiparesis. *J Magn Reson Imaging* 2003;18:641–48
- Lee ZI, Byun WM, Jang SH, et al. Diffusion tensor magnetic resonance imaging of microstructural abnormalities in children with brain injury. *Am J Phys Med Rehabil* 2003;82:556–59
- Thomas B, Elyssen M, Peeters R, et al. Quantitative diffusion tensor imaging in cerebral palsy due to periventricular white matter imaging. *Brain* 2005;128:2562–77
- Hoon AH Jr, Lawrie WT Jr, Melhem ER, et al. Diffusion tensor imaging of periventricular leukomalacia shows affected sensory cortex white matter pathways. *Neurology* 2002;59:752–56
- Fan GG, Yu B, Quan SM, et al. Potential of diffusion tensor MRI in the assessment of periventricular leukomalacia. *Clin Radiol* 2006;61:358–64
- Anjari M, Srinivasan L, Allsop JM, et al. Diffusion tensor imaging with tract-based spatial statistics reveals local white matter abnormalities in preterm infants. *Neuroimage* 2007;35:1021–27. Epub 2007 Feb 8.
- Jones DK, Horsfield MA, Simmons A. Optimal strategies for measuring diffusion in anisotropic systems by magnetic resonance imaging. *Magn Reson Med* 1999;42:515–25
- Woods RP, Cherry SR, Mazziotta JC. Rapid automated algorithm for aligning and reslicing PET images. *J Comput Assist Tomogr* 1992;16:620–33
- Makris N, Worth AJ, Sorensen AG, et al. Morphometry of in vivo human white matter association pathways with diffusion-weighted magnetic resonance imaging. *Ann Neurol* 1997;42:951–62
- Pierpaoli C, Basser PJ. Toward a quantitative assessment of diffusion anisotropy. *Magn Reson Med* 1996;36:893–906
- Pajevic S, Pierpaoli C. Color schemes to represent the orientation of anisotropic tissues from diffusion tensor data: application to white matter fiber tract mapping in the human brain. *Magn Reson Med* 1999;42:526–40
- Stieltjes B, Kaufmann WE, van Zijl PC, et al. Diffusion tensor imaging and axonal tracking in the human brainstem. *Neuroimage* 2001;14:723–35
- Wakana S, Jiang H, Nagae-Poetscher LM, et al. Fiber tract-based atlas of human white matter anatomy. *Radiology* 2004;230:77–87
- Mori S, van Zijl PC. Fiber tracking: principles and strategies—a technical review. *NMR Biomed* 2002;15:468–80
- Catani M, Howard RJ, Pajevic S, et al. Virtual in vivo interactive dissection of white matter fasciculi in the human brain. *Neuroimage* 2002;17:77–94
- Mori S, Crain BJ, Chacko VP, et al. Three-dimensional tracking of axonal projections in the brain by magnetic resonance imaging. *Ann Neurol* 1999;45:265–69
- Conturo TE, Lori NF, Cull TS, et al. Tracking neuronal fiber pathways in the living human brain. *Proc Natl Acad Sci U S A* 1999;96:10422–27
- Huang H, Zhang J, van Zijl PC, et al. Analysis of noise effects on DTI-based tractography using the brute-force and multi-ROI approach. *Magn Reson Med* 2004;52:559–65
- Maenpaa H, Salokorpi T, Jaakkola R, et al. Follow-up of children with cerebral palsy after selective posterior rhizotomy with intensive physiotherapy or physiotherapy alone. *Neuropediatrics* 2003;34:67–71
- Chang CH, Albarracín JP, Lipton GE, et al. Long-term follow-up of surgery for equinovarus foot deformity in children with cerebral palsy. *J Pediatr Orthop* 2002;22:792–99
- Bartlett DJ, Palisano RJ. Physical therapists' perceptions of factors influencing the acquisition of motor abilities of children with cerebral palsy: implications for clinical reasoning. *Phys Ther* 2002;82:237–48
- Krach LE. Pharmacotherapy of spasticity: oral medications and intrathecal baclofen. *J Child Neurol* 2001;16:31–36
- Arzoumanian Y, Mirmiran M, Barnes PD, et al. Diffusion tensor brain imaging findings at term-equivalent age may predict neurologic abnormalities in low birth weight preterm infants. *AJNR Am J Neuroradiol* 2003;24:1646–53
- Liao D, Cooper L, Cai J, et al. Presence and severity of cerebral white matter lesions and hypertension, its treatment, and its control: The ARIC Study—Atherosclerosis Risk in Communities Study *Stroke* 1996;27:2262–70
- Loes DJ, Hite S, Moser H, et al. Adrenoleukodystrophy: a scoring method for brain MR observations. *AJNR Am J Neuroradiol* 1994;15:1761–66
- Simon EM, Hevner R, Pinter JD, et al. Assessment of the deep gray nuclei in holoprosencephaly. *AJNR Am J Neuroradiol* 2000;21:1955–61
- Okoshi Y, Itoh M, Takashima S. Characteristic neuropathology and plasticity in periventricular leukomalacia. *Pediatr Neurol* 2001;25:221–26
- Davatzikos C, Barzi A, Lawrie T, et al. Correlation of corpus callosal morphometry with cognitive and motor function in periventricular leukomalacia. *Neuropediatrics* 2003;34:247–52
- Baker LL, Stevenson DK, Enzmann DR. End-stage periventricular leukomalacia: MR evaluation. *Radiology* 1988;168:809–15
- Flodmark O, Roland EH, Hill A, et al. Periventricular leukomalacia: radiologic diagnosis. *Radiology* 1987;162(1 Pt 1):119–24
- Flodmark O, Lupton B, Li D, et al. MR imaging of periventricular leukomalacia in childhood. *AJR Am J Roentgenol* 1989;152:583–90
- Truwit CL, Barkovich AJ, Koch TK, et al. Cerebral palsy: MR findings in 40 patients. *AJNR Am J Neuroradiol* 1992;13:67–78
- Xue R, van Zijl PC, Crain BJ, et al. In vivo three-dimensional reconstruction of rat brain axonal projections by diffusion tensor imaging. *Magn Reson Med* 1999;42:1123–27
- Mori S, Kaufmann WE, Davatzikos C, et al. Imaging cortical association tracts in the human brain using diffusion-tensor-based axonal tracking. *Magn Reson Med* 2002;47:215–23